Available online at www.sciencedirect.com
ScienceDirect
Journal of the European Ceramic Society 27 (2007) 3573–3588
www.elsevier.com/locate/jeurceramsoc

Corrosion of Si_3N_4-ceramics in aqueous solutions Part 2. Corrosion mechanisms in acids as a function of concentration, temperature and composition

J. Schilm, M. Herrmann *, G. Michael

Fraunhofer Institute for Ceramic Technologies and Systems, Winterbergstr. 28, 01277 Dresden, Germany

Received 28 November 2005; received in revised form 2 May 2006; accepted 6 May 2006
Available online 11 April 2007

Abstract

The corrosion behaviour of Si_3N_4-ceramics with different grain boundary compositions was investigated in H_2SO_4 with different concentrations at 90 °C and was compared with the corrosion behaviour of glasses. In part I of this paper the influence of temperature was investigated [Schilm, J., Gruner, W., Herrmann, M. and Michel, G. Corrosion of Si3N4-ceramics in aqueous solutions, J. Eur. Ceram. Soc., 26 (2006) 3909–3917] The investigation showed that the corrosion rate as well as the corrosion mechanisms strongly depend on the concentration and temperature of the acid and the composition of the grain boundary phase. The observed dependencies allow the prediction of the corrosion behaviour of silicon nitride ceramics in acids. The investigation of the morphology of the corrosion layers by SEM and TEM proves that the observed passivation of the materials during corrosion in H_2SO_4 with concentrations higher than 0.5 mol/l is caused by the formation of SiO_2-rich layers inside the corroded triple junctions.

The experimental results were discussed in terms of corrosion mechanisms allowing a qualitative prediction of the corrosion behaviour at least. The corrosion resistant Si_3N_4-materials can be reached by tailoring the amount and composition of the grain boundary phase.

Keywords: Silicon nitride; Aqueous corrosion; Microstructure

1. Introduction

Silicon nitride materials are one of the most prominent structural ceramics and are applied in areas in which properties like high strength, fracture toughness, hardness and corrosion resistance are necessary, such as ball bearings, cutting tools, parts in heat combustion engines. In addition to silicon nitride grains silicon nitride materials contain the grain boundary formed by the sintering additives and the SiO_2, existing on the surface of the starting Si_3N_4-powder. The corrosion resistance of Si_3N_4 materials in acids strongly depends on the composition of the grain boundary phase, especially on the SiO_2 content of the grain boundary phase.[1–6] The systematic investigation of the influence of the grain boundary composition on the corrosion resistance in 0.5 mol/l H_2SO_4 was the main topic of the first part of the articles.[1] The subject of the second part of this study is the evaluation of the corrosion behaviour of selected Si_3N_4 ceramics characterized in the first part (Table 1) in acidic environments with different concentrations.[1] Additionally the corrosion behaviour of two oxynitride glasses was tested. The details of the preparation are given in Ref. 7.

2. Experimental

Series of materials were produced with a systematic variation of the sintering additives. The compositions are given in Table 1. Details of the compositions, starting powders, preparation and methods of analysis of the ceramics and glasses are given in part 1.[1] The mean width of the grains was in the range of 0.5–0.7 μm. Typical microstructures are given in Fig. 1. As was shown in part I, more than 95% of the grain boundary phase is concentrated in the triple junctions for materials with more than 5 vol.% grain boundary phases. The volume content of the grain boundary can only be approximated due to the unknown density of the grain boundary. Assuming a density of 4 g/cm^3 which was observed for oxynitride glasses of similar compositions the volume fraction of the grain boundary is approximately

* Corresponding author.
E-mail address: herrmann@ikts.fhg.de (M. Herrmann).

0955-2219/$ – see front matter © 2006 Elsevier Ltd. All rights reserved.
doi:10.1016/j.jeurceramsoc.2006.05.082

Table 1
Compositions of the grain boundary phases of all Si_3N_4 materials after sintering calculated with respect to the mass content of the grain boundaries and of the two investigated glasses

Material	Amount of grain boundary phase (mass%)	Compositions of the grain boundary phases calculated from the oxygen distributions in the sintered ceramics[1]					
		SiO_2 (mol%)	Al_2O_3 (mol%)	Y_2O_3 (mol%)	Si_3N_4[a] (mol%)	MgO (mol%)	X
KORSiN 4	9.8	43.0 ± 2.5	15.0 ± 2.0	35.0 ± 1.6	7.0		1.38
KORSiN 2a	12.6	57.0 ± 1.8	13.1 ± 1.4	23.0 ± 0.9	7.0		2.45
KORSiN 5	17.9	54.5 ± 1.0	17.0 ± 0.8	21.5 ± 0.6	7.0		2.57
KORSiN 6	14.6	62.3 ± 1.5	12.2 ± 1.2	18.5 ± 0.7	7.0		2.80
KORSiN 8	13.7	60.0 ± 1.6	12.8 ± 1.3	20.2 ± 0.7	7.0		2.68
KORSiN 9	14.3	61.2 ± 1.5	12.8 ± 1.3	19.0 ± 0.6	7.0		2.76
KORSiN 7	10.1	74.8 ± 1.7	1.8 ± 1.5	18.3 ± 0.8	7.0		2.80
SN0	11.9	52.3 ± 2.0	15.2 ± 1.6	25.5 ± 1.0	7.0		2.26
SN3	10.8	50.4 ± 2.2	13.0 ± 1.7	29.6 ± 1.3	7.0		1.90
SN2	4.4	75.2 ± 0.5	0.1	4.5 ± 0.1	7.0	13.3 ± 0.3	3.43
Glass GLAY8[b]		50.0	25.0	20.0	5.0		2.61
Glass GLAY13[c]		57.0	30.0	10.0	3.0		3.25

[a] Assumed as 17 eq.% N.
[b] Oxynitride glasses
[c] X-numbers of bridging anions: $X = 8 - 2 \cdot ([O] + [N]/[Si] + (2/3)[Al])$; [O], [N], [Si] and [Al] are concentrations in atom%.

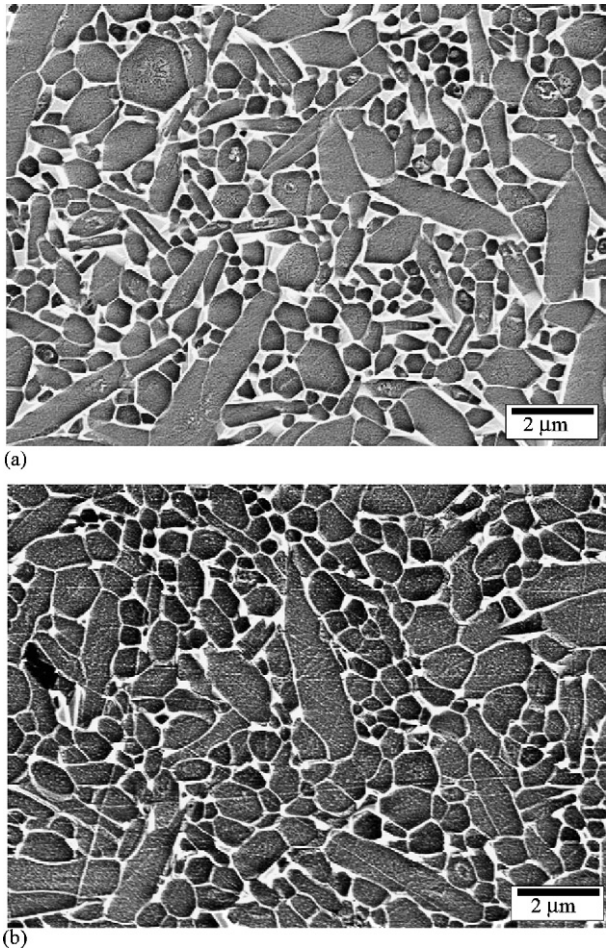

Fig. 1. FESEM-micrographs of polished etched sections of the materials SN3 (a) and SN2 (b).

80% of the weight fraction i.e. less rhan 15 vol.%. The mean area of the triple junctions was in the range of 0.04–0.06 μm^2 for the different materials.[5]

All corrosion tests were carried out in a 1.5-l Teflon reaction vessel equipped with Teflon sample holders. The test samples were plates with dimensions 16 mm × 16 mm × 2.5 mm. The ratio between the surface of the samples and the volume of the acid was lower than 0.005 m^{-1}. The solutions were continuously stirred and completely changed after certain times to avoid a strong enrichment of dissolved glass components. This setup is necessary to avoid experimental disadvantages which have been found in the reviewed literature. A thermostat filled with silicone oil was used to heat the vessel. The requested temperature was maintained within a range of ±0.5 K.

The standard preparation procedure before and after all corrosion experiments was to wash the samples in acetone for 10 min, to rinse them with deionised water, to dry them for ≥2 h at 150 °C and to weigh them on a microbalance ($\Delta m = 0.01$ mg) after a 2 h cooling period.

Cross sections of the corroded samples were investigated by optical microscopy and SEM. Corrosion indicators like the thickness of corroded layers were evaluated by quantitative image analysis (Image Tool v3). The thickness of the corrosion layer was measured on cross sections as an average of the area of the layer divided by the length of the measured window. The typical errors of determination of the thicknesses were less 15% for thicknesses of up to 50 μm and less than 5% for the thicker corrosion layers.

In all figures the thickness of the corrosion layer is the thickness of the whole layer and not the thickness of sublayers. The chemical composition across the corrosion layers were analyzed by EDX. Therefore, the samples were coated with carbon. Selected samples were analyzed by TEM.

The strength was measured on bending bars 3 mm × 4 mm × 45 mm in four-point bending (fixtures: 40/20 mm loading rate 0.5 mm min^{-1}).

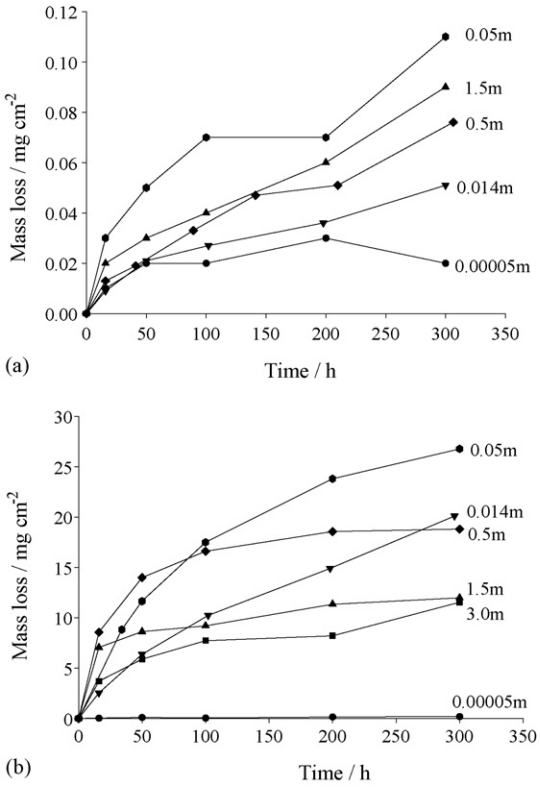

Fig. 2. Dependence of the corrosion of SN2 (weight gain (a) thickness of the corrosion layer (b) and SN3 (c) on the corrosion time in sulphuric acid with different concentrations (in mol/l) at 90 °C.

3. Results

3.1. Corrosion of ceramics and oxynitride glasses in H_2SO_4 of different concentrations

The materials SN3 (Y_2O_3/Al_2O_3 sintering additives) and SN2 ($MgO/Y_2O_3/Al_2O_3$ sintering additives) with different compositions and amount of grain boundary phases were corroded in H_2SO_4 at 90 °C in a concentration range between 0.00005 and 3 mol/l (Fig. 2). Bending bars were chosen for these experiments to receive additional information about the residual bending strength of the materials.

Material SN2, which has a grain boundary phase that is very stable in acids, exhibited only a small increase of weight loss and no significant change in the character of the overall corrosion behaviour with changing H_2SO_4 concentrations. Even after 300 h of corrosion the mass losses vary only between 0.02 and 0.11 mg cm^{-2}. Due to small mass losses, changes in the corrosion mechanism are rather hardly recognizable. Nevertheless, in this material there is also the tendency that the corrosion in 0.05 mol/l H_2SO_4 is stronger than in more concentrated and more diluted acids. The residual bending strength of SN2 samples after corrosion in 0.00005 mol/l acid did not significantly changed in comparison to the initial strength (Table 2) which can be correlated with the low mass losses in this medium. In the more concentrated solutions the residual strength was reduced by ≈150 MPa compared to the original value (Table 2). This was found despite the fact that no corrosion layer was observed, indicating local pit formation.

A strong dependence of the corrosion kinetics on the concentration of H_2SO_4 was observed for the material SN3. Except for a 0.00005 mol/l sulphuric acid the measured mass losses were 1000 times greater than those of the material SN2. At a H_2SO_4 concentration of 0.00005 mol/l the mass loss after 300 h of corrosion reached 0.18 mg cm^{-2}. This small mass loss was accompanied by a reduction of the bending strength from 985 MPa in the initial state to 819 MPa (Table 2).

At higher concentrations of the acid the observed mass losses increased strongly and the time dependent plots had significant curvatures. During corrosion in 0.5 mol/l H_2SO_4, SN3 exhibited a pronounced passivation behaviour as described in the first part of the paper for materials with similar composition.[1] A similar behaviour like in 0.5 mol/l H_2SO_4 was observed in acids with higher concentrations (1.5 and 3 mol/l). Despite the higher initial dissolution rates up to 10–16 h the passivation in concentrated H_2SO_4 occurs after shorter corrosion times and at significant lower mass loss levels. The consequence of this behaviour was the increased stability with increasing concentration of the acid (Figs. 2 and 3).

The residual bending strength of the SN3 samples after 300 h corrosion in 0.014–3 mol/l sulphuric acid dropped to 470 and 600 MPa (Table 2). The lowest residual strength was observed for the samples corroded in 0.5 mol/l H_2SO_4. This corresponds with the mass losses of the samples.

Oxynitride glasses of compositions that are similar to the grain boundaries of the Si_3N_4-materials investigated in this paper, showed linear corrosion kinetics for both the mass loss

Table 2
Residual strength and thickness of the corrosion layer after 300 h corrosion in H_2SO_4 with different concentration

Concentration (mol/l)	Residual bending strength (MPa)		Thickness of the corrosion layer (μm)
	SN2	SN3	SN3
	847 ± 103[a]	985 ± 22[a]	–
0.00005	791 ± 69	819 ± 18	<10
0.014	702 ± 104	593 ± 43	755
0.05	702 ± 40	470 ± 55	1250
0.5	732 ± 41	547 ± 16	1390
1.5	693 ± 53	520 ± 44	630
3	–	605 ± 30	600

SN2 shows only some pittings on the surfaces of the samples but no measurable thickness of the corrosion layers.
[a] Initial values.

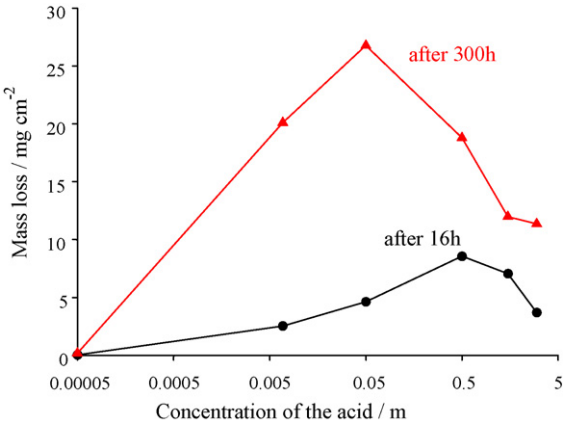

Fig. 3. Dependence of the weight losses during corrosion at 90 °C as a function of the concentration of the acid after 16 and 300 h corrosion time.

and the changes of the dimensions in 0.5 mol/l H_2SO_4 at 90 °C as demonstrated in the previous publication.[7] In Figs. 4 and 5, the behaviour of two glasses with different silica contents is shown. In 0.05 mol/l and in 3 mol/l H_2SO_4 at 90 °C linear time dependencies of the weight loss and of the reduction in thickness were observed at least for corrosion times higher than 5 h (Figs. 4 and 5). The SiO_2 rich glass GLAY13 is more stable in H_2SO_4 than the glass GLAY8. With a rising concentration of the acid, the corrosion rate of the less stable glass GLAY8 increases. For the relatively stable glass GLAY13 the corrosion rate in 3 mol/l H_2SO_4 is much lower than in 1N H_2SO_4. This is an evidence for passivating mechanisms.

Fig. 6a–d shows SEM images of glass sample GLAY8 and GLAY13 after corrosion in 0.05 and 3 mol/l H_2SO_4. The appearance of broad and flat pits on the surface after corrosion of the glasses is typical for the corrosion in 0.5 mol/l H_2SO_4 (Fig. 6a and c). This feature is also known from the corrosion of other glasses in aqueous media. Under these conditions the corrosion leads to a complete dissolution of the glass network without any layers as shown by EDX. Also additional XRD analyses of the corroded sample gave no hints for crystallized products.

The corrosion rate of the more SiO_2 rich glass GLAY13 in 0.5 mol/l H_2SO_4 is higher than in diluted and concentrated H_2SO_4. The reason for the reduced corrosion rate in 3 mol/l H_2SO_4 is the formation of a SiO_2 rich surface layer (Fig. 6d). This was shown by EDX-analyses of the corroded surface. The analyses reveal a strong enrichment of silica compared to the original composition of GLAY13. The deposited SiO_2 layer has a very high roughness as seen in Fig. 6d. The amorphous structure of this layer was proven by XRD. Such a corrosion layer was not observed after corrosion of GLAY13 in 0.5 mol/l H_2SO_4 at 90 °C. In 3 mol/l H_2SO_4 also GLAY8 showed a different surface morphology compared to the observations made after treatment in 0.5 mol/l H_2SO_4. By means of EDX analyses small and isolated deposits on the surface were identified as SiO_2 rich particles. After corrosion in 0.05 mol/l H_2SO_4 only isolated SiO_2-rich deposits could be observed on the surfaces of GLAY13 samples but no continuous layer as after corrosion in 3 mol/l H_2SO_4.

These results suggest that the observed passivation during corrosion of the Si_3N_4 materials is connected with the formation of SiO_2 rich layers. Therefore, the morphologies of the corrosion layers of the material SN3 were investigated more detailed (see Section 3.3).

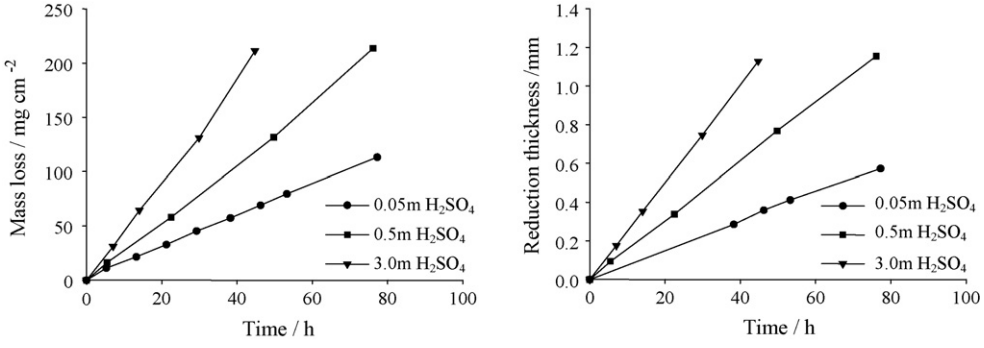

Fig. 4. Mass loss and reduction in the thickness during corrosion of the glass GLAY8 in 0.05, 0.5, and 3.0 mol/l H_2SO_4 at 90 °C.

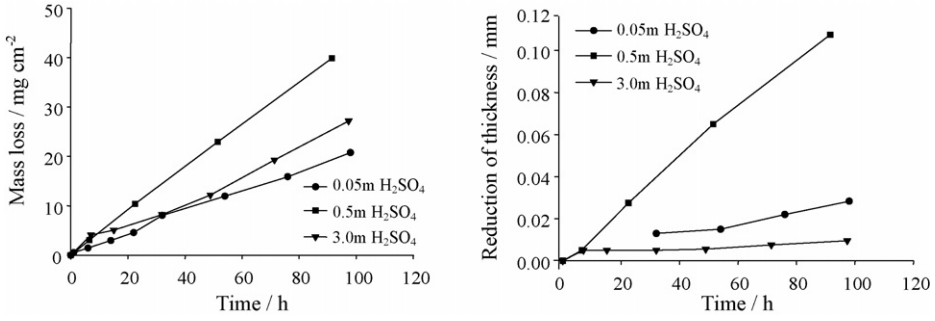

Fig. 5. Mass loss and reduction in the thickness during corrosion of the glass GLAY13 in 0.05, 0.5, and 3.0 mol/l H_2SO_4 at 90 °C.

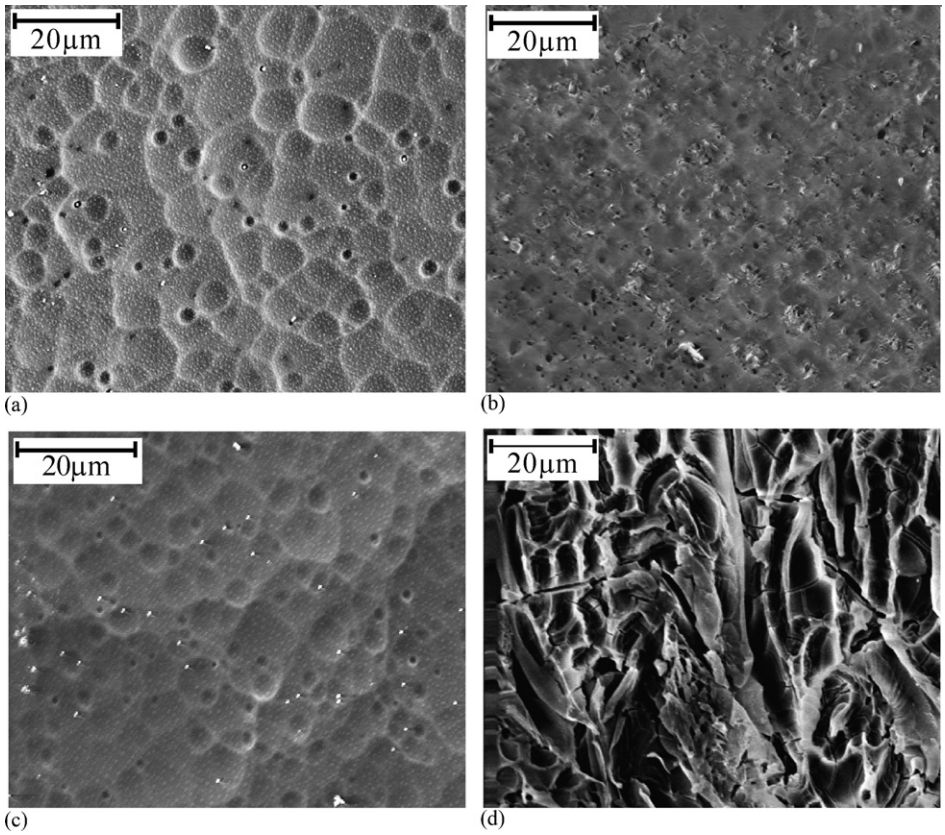

Fig. 6. SEM micrographs of GLAY8 (a and b) and GLAY13 (c and d) after corrosion in 0.5 mol/l H_2SO_4 (a and c) and in 3 mol/l H_2SO_4 (b and d) at 90 °C after (70 h).

3.2. Analysis of the eluate during corrosion

The corrosion behaviour of the material SN3 was also investigated by measuring the concentration of the dissolved ions by ICP/AES. The results of the eluate measurements are given in Fig. 7. Beside the values measured, the data of the concentrations calculated from the thickness of the corrosion layer and the composition of the grain boundary are given.

The values calculated for Y_2O_3 match perfectly the measured data. The measured concentrations of Al_2O_3 is slightly higher than the calculated ones by the dissolution of the grain boundary. This could be connected with slightly too high z values determined or with some dissolution of Si_3N_4 grains. The discrepancies between the measured and calculated data are much higher for the SiO_2 content. In the period up to 25 h the measured values show the tendency of higher values in comparison to the calculated ones. For longer corrosion times less SiO_2 was measured than expected based on the composition of the grain boundary. This is an indication that the SiO_2 of the grain boundary was not completely dissolved during the long-term experiments. This process can be schematically described by the following equation:

$$SiO_2(\text{glass}) + nH_2O \rightarrow SiO_2{\cdot}nH_2O \quad (1)$$

The measured weight losses and the calculated weight losses based on the concentrations of the components in the eluate are shown in Fig. 7b. It is obvious that more components than expected from the weight loss are leached out. This can be caused by the partial hydrolysis of the Si_3N_4 grains by the reaction:

$$Si_3N_4 + 3(n+2)H_2O + 4H^+ \rightarrow 3SiO_2{\cdot}nH_2O + 4NH_4{}^+ \quad (2)$$

The formed SiO_2 only partially dissolves in the solution. The formation of precipitated in the triple junctions $SiO_2{\cdot}nH_2O$ results in weight gain. This compensates the weight losses due to leaching. Corrosion rates of 10^{-16} cm^2/h (parabolic rate constant), as observed for the hydrolysis of Si_3N_4 powders in water at 100 °C,[9] result in the reduction of grain sizes of approximately 1 nm in 100 h. Considering the high specific surface area of the corroded layer, this hydrolysis could be a source for the discrepancy of the weight losses, and the measured concentration (reaction (2) result in weight gain).

Detailed investigations of the corrosion layer were carried out to prove these findings.

3.3. Morphology of the corrosion layers

In Fig. 8, the mass loss of the material SN3 normalised on the corroded volume is given as a function of time for the corrosion in 0.5 and 0.05 mol/l H_2SO_4 at 90 °C. The data were calculated by the ratio of mass loss and the volume of the corrosion layer. They characterize the amount of the grain boundary phase that is leached from the unit corroded volume. It is clearly recognized that the grain boundaries were more completely leached by 0.05 mol/l H_2SO_4 than by 0.5 mol/l H_2SO_4. On the other

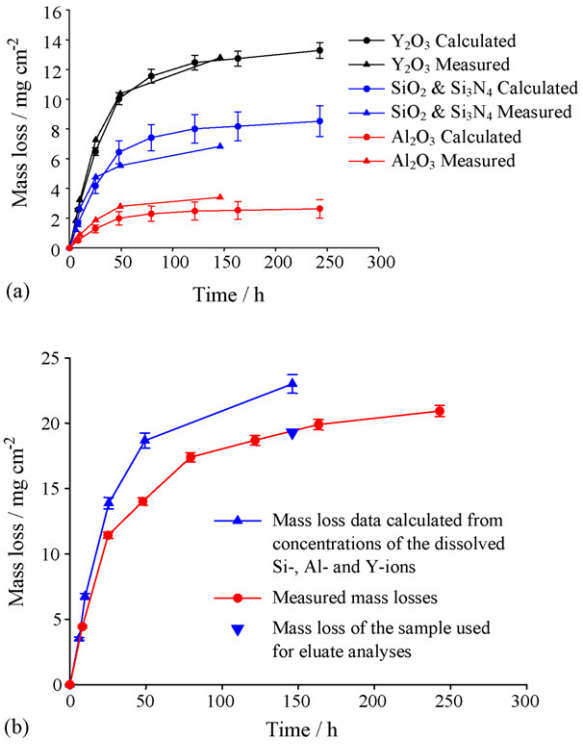

Fig. 7. (a) Concentration of Y, Al and Si in the solution as a function of corrosion time of SN3 in 0.5 mol/l H_2SO_4 at 90 °C; the original concentrations were recalculated in the weight of oxide solved. Additionally concentrations are given, which were calculated on the basis of the composition of the grain boundary and the thickness of the corrosion layer; (b) weight loss data calculated from concentrations of the dissolved ions in comparison with the measured weight losses.

side the values observed for 0.05 mol/l H_2SO_4 agreed with the amount of grain boundary existing in the uncorroded sample (350 ± 5 mg/cm^3) values were calculated using the mass content of grain boundary (Table 1) and the density of the material 3.243 g/cm^3).[1]

These results reveal that components of the grain boundary phases must remain inside the corroded triple junctions

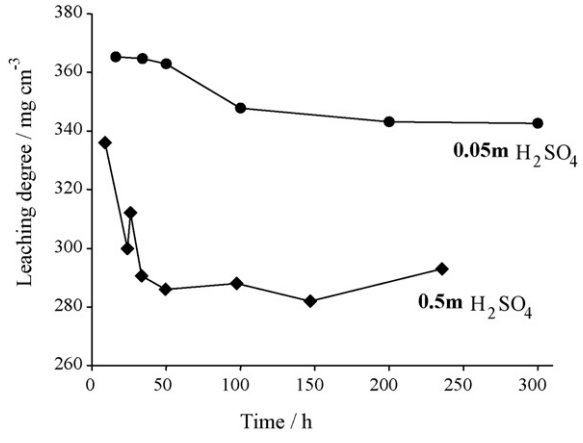

Fig. 8. Leaching degrees of SN3 in 1.0 and in 0.1N H_2SO_4 at 90 °C as a function of corrosion time.

in the case of corrosion in sulphuric acid with concentration ≥0.5 mol/l. This could be confirmed by analysing the cross sections of the corroded samples (Fig. 9). The observation of the corrosion layers using a stereomicroscope revealed the existence of at least two different sublayers when a certain thickness of the corrosion layer has been reached. These sublayers were identified independently from the corrosion conditions with light microscope. As an example the morphology of the corrosion layers of SN3 at 90 °C in H_2SO_4 with different concentrations are depicted in Fig. 9. It can be recognized that the formation of the inner, light shaded layer occurs after the strong reduction of the corrosion rate. As far as we aware these conditions are given at temperatures of at least 90 °C in acids of a 1 mol/l or even higher proton concentration.

Single corrosion layers or double layers with a less pronounced transformation in the corrosion kinetic were observed in samples which were corroded in more diluted acids (<1 mol/l proton concentration) at temperatures of 90 °C and at lower temperatures in acids with 1 mol/l proton concentration. Similar behaviour was observed by Schilm[3,5] and Seipel[6,8] before. It has to be mentioned that even very small changes of the refractive index on the surface of an observed sample can be seen clearly using light microscope. Such changes in the refractive index can be caused by smallest silicatic depositions inside the corroded triple junctions. Unfortunately, this effect cannot be used to judge even qualitatively about the amounts of deposited silica.

A more detailed examination of the layers by scanning electron microscopy revealed clearly, that the outer corrosion layer has a greater porosity than the inner layer (Fig. 10). The EDX analysis discovered higher oxygen content of the inner corrosion layer in comparison to the composition of the outer layer. These results can be taken as a hint for hydrated silicatic deposits in the corroded triple junctions and some hydrolysis of the Si_3N_4-grains. It was also determined qualitatively by EDX analysis that the extent of the enrichment and the density of these silicatic deposits depends significantly on the corrosion conditions and the thickness of the corrosion layer. In the case of passivation during corrosion in the inner corrosion layers an higher oxygen content could be observed. Under corrosion conditions, where no changes in the corrosion mechanisms were observed, no significant increase of oxygen concentration was observed, proving a less amount of precipitated $SiO_2 \cdot nH_2O$. In the sample SN3 leached in 0.05 mol/l H_2SO_4 such differences in porosity and oxygen content could not be observed.

It is also visible that Al is only partially dissolved during the corrosion. This correlates with the amount of Al incorporated in the Si_3N_4-lattice.

TEM investigations of the corroded microstructures of samples SN3 confirm these findings.[10] The TEM images (Fig. 11b–d) showed corroded triple junction with deposits in the triple junctions especially at the grain edges. It was observed by EDX that the deposits consist mainly of silicon and oxygen. The TEM investigations confirm an amorphous state of the silicatic deposits. The TEM-examination of the outer layer (Fig. 11b) revealed that only very thin hydrated layers on the surface of the Si_3N_4 grains exist in this region.

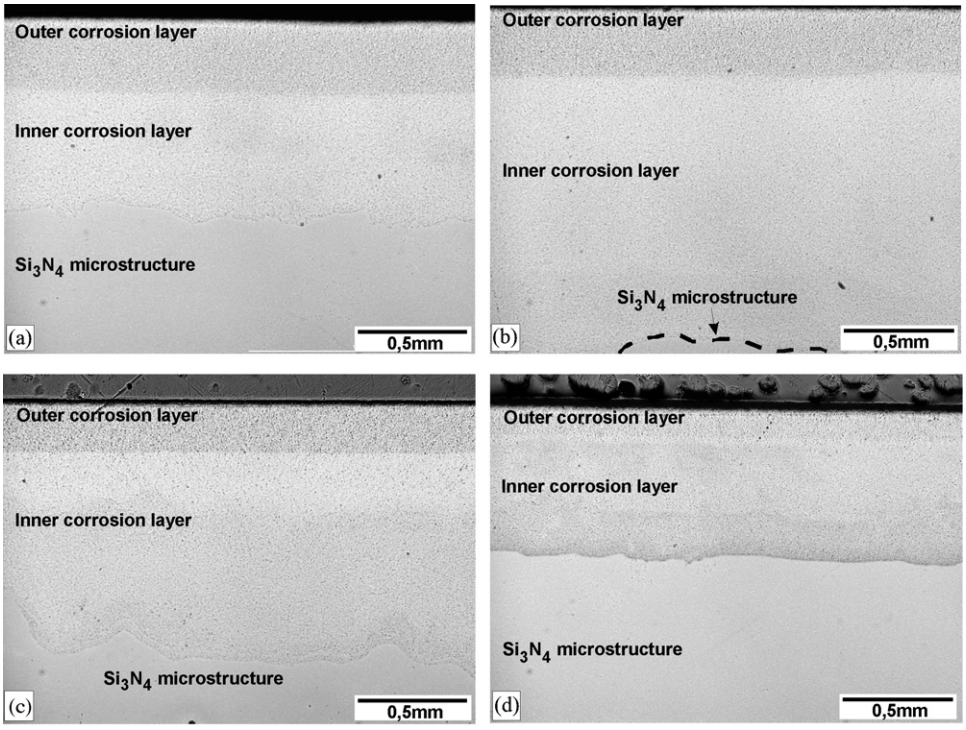

Fig. 9. Optical micrographs of the material SN3 after corrosion in H_2SO_4 with different concentrations after 300 h at 90 °C; (a) 0.014 mol/l H_2SO_4, (b) 0.05 mol/l H_2SO_4, (c) 0.5 mol/l H_2SO_4 and (d) 3.0 mol/l H_2SO_4.

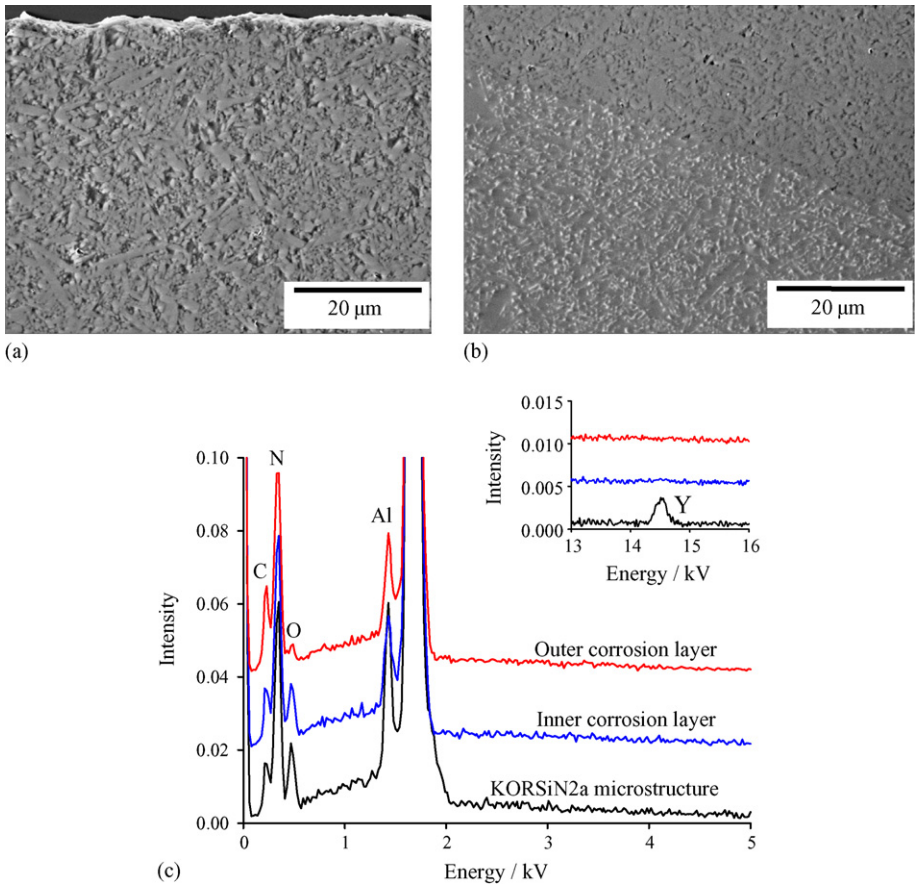

Fig. 10. SEM image of the outer corrosion layer (a) and the inner corrosion layer (b) of KORSiN2a and results of EDX-analysis (c) after corrosion in 0.5 mol/l H_2SO_4 at 90 °C for 220 h (polished cross section).

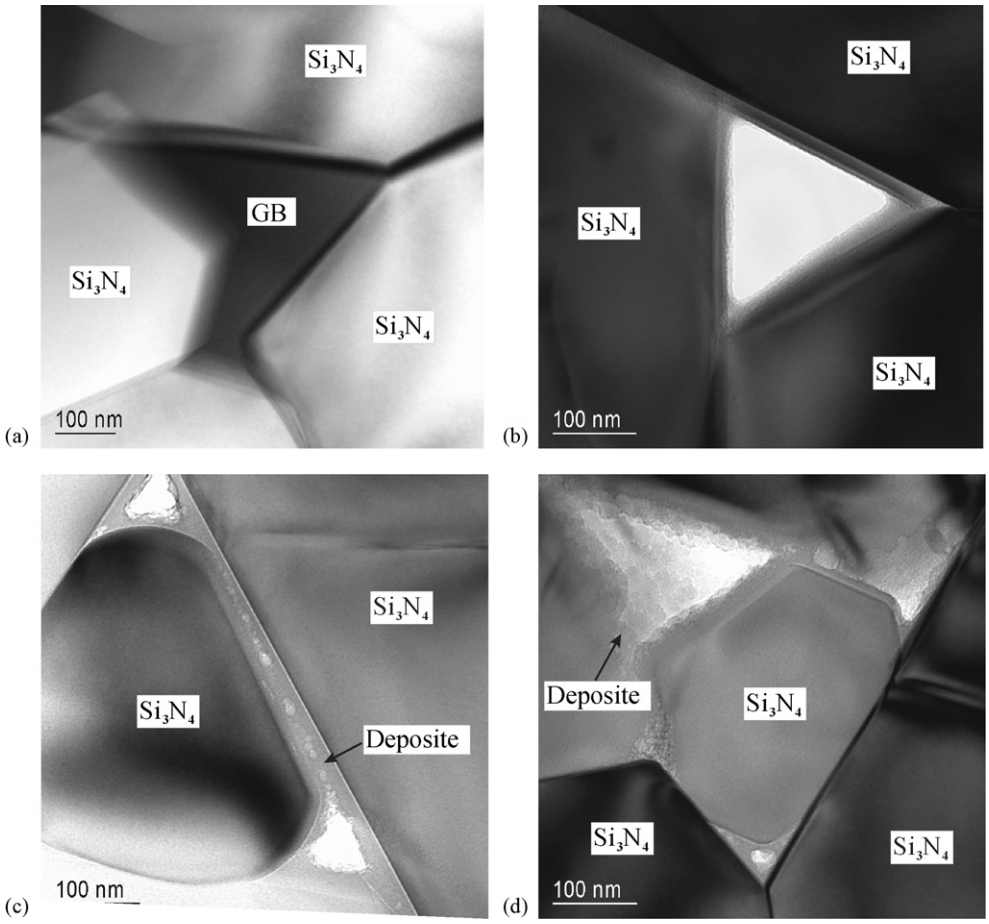

Fig. 11. TEM-micrographs of the material SN3: (a) uncorroded samples (b) outer corrosion layer, (c) and (d) inner corrosion layer. The deposition of SiO_2 reach remaining grain boundary was observed in the inner corrosion layer (GB—grain boundary).

4. Discussion

4.1. Corrosion mechanism

4.1.1. Overall figures

The corrosion process of the Si_3N_4-materials is influenced by different processes. At first, it is caused by transport process from the solution to the surface of the material. This process is not discussed in this article and its influence is minimised by the experimental set up.

Secondly, there are the chemical processes resulting in the dissolution of the grain boundaries and the grains. These processes are strongly dependent on the acid concentration and the composition of the grain boundary. They are decisive in the beginning of the corrosion (linear corrosion rates).

With the formation of the corrosion layer of several hundred μm, additional processes take place which can determine the corrosion under certain conditions. These processes are connected with the formed pore structure of the corrosion layer. The typical pore channels are in the range of 1 μm or less.

The overall analyses of the experimental results show that the corrosion rate of the grain boundary phase in silicon nitride ceramics is commonly higher than the corrosion of the grains. Therefore, the corrosion behaviour of silicon nitride ceramics mainly depends on the amount and composition of the grain boundary phase which forms a three-dimensional skeleton, even at a low additive contents (see for example[4]). The low corrosion of the grains in comparison to the grain boundary phase is in agreement with the corrosion rates of less than 10^{-16} cm^2/h (parabolic rate constant) observed for the hydrolysis of Si_3N_4 powder in water at 100 °C[2,9] and the much higher values observed for oxynitride glasses with compositions similar to the grain boundaries[1,5,7]. Therefore, the grains and the thin films between the grains show only a minor attack during corrosion in acids (Fig. 11) at least up to 130 °C (excluding HF)[15] resulting in the observed very strong corrosion layers (corroded porous material shows still a four point bending strength of 400 MPa).[4,5,11]

The reason for the different corrosion rates of the nm thick grain boundary films between the grains and the triple junctions could be caused by kinetic factors. Thin SiO_2-films were observed at the surface of the Si_3N_4 grains in the corrosion layer (Fig. 11) which do not only reduce the dissolution of the Si_3N_4 grains but also protect the thin films between the Si_3N_4 grains from further corrosion. Additionally, it could be caused by the different compositions of these two regions. TEM-investigations and theoretical models[12–14] indicate that the thin films at least for Y-containing glasses are richer in SiO_2 and Si_3N_4 in com-

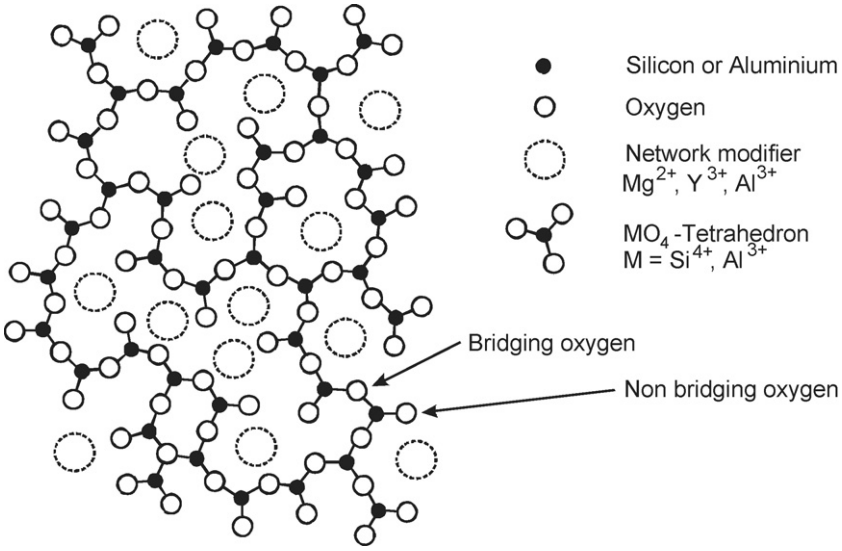

Fig. 12. Simplified two-dimensional model of a silicatic glass structure illustrating the roles of network-forming and network-breaking cations in an amorphous glass network.

parison to the triple junctions. The consequence of the stability of the thin grain boundary films in H_2SO_4, HCl, HNO_3, H_3PO_4, and other mineral acids is the high stability of the corrosion layer. In F^--containing solutions (HF or florid containing other acids)[15] SiO_2-rich compounds are unstable due to the ability of F^- ions to dissolve SiO_2. Therefore, HF dissolves both grains and the thin grain boundary films resulting in changed corrosion behaviour in comparison to the corrosion behaviour in other mineral acids.[15,21]

The different corrosion rates observed for the grains and the grain boundary phase (triple junctions) result in initial linear corrosion rates of the Si_3N_4 materials, which can be directly correlated with the stability of the amorphous grain boundary phase (Figs. 11 and 12 in Part 1[1,4]).

The reduced transport of the reaction products and reactants through pores and their interaction with the walls of the pores (the surface of the Si_3N_4 grains) can result in the formation of a passivating layer which leads to a strong reduction of the corrosion rate. These processes depend on the rate of the dissolution of the grain boundary, the pore structure and the corrosion conditions.

A more detailed analysis of the chemical processes has to be done to understand the influence of the composition and the corrosion conditions on the dissolution of the grain boundary phase and the formation of the passivating layers. This is the topic of the next chapter.

4.1.2. Dissolution of the grain boundary phase and formation of protecting layers

Materials with grain boundary phases which are SiO_2 rich show a high stability. The reasons for this correlation can be derived from principles of glass science.

The structure of a glass network and the properties of glasses can be described by the value X – the number of bridging anions (Z) per network-forming cation M (see Table 1).[1,16–18] The network is formed by MZ_4-tetrahedra containing silica and alumina as cations. Alumina is only to a certain extent a network-forming component of the glass network. Other components forming bonds with dominantly ionic character such as yttrium, magnesium or calcium are considered as network modifiers which produce non-bridging oxygen atoms (Fig. 12). The glass network is stronger, if the amount of bridging anions is higher (e.g. in SiO_2 glasses only bridging anions exist $X=4$). This is also the reason why the glass network is strengthened with nitrogen incorporation (3-bonds/atom) or softened with the incorporation of Cl^- or OH^- (only non-bridging anion).

Corrosion of glass in acids can be described by the leaching of the network modifier (in our case Y, Mg and particular Al) and formation of a hydrated glass network in the first step. Schematically this can be illustrated by the following reaction (this reaction is the more complex expression of reaction (1) explaining the leaching of the network modifiers):

$$\equiv (\text{Si–O})_n\text{–M} + n\text{H}_{(\text{aqu.})}{}^{+} \rightarrow n \equiv \text{Si–OH} + \text{M}_{(\text{aqu.})}{}^{n+} \quad (3)$$

For longer corrosion times the outward diffusion of the cations M^{n+} through the formed layer of the hydrated network becomes slower and slower and the dissolution of the hydrated network becomes rate-controlling.[16] This dissolution is shown schematically in the reaction:

$$\equiv \text{Si–O–SiO}_{2-n}(\text{OH})_n + \text{H}_2\text{O} \rightarrow \equiv \text{Si–OH} + \text{SiO}_{2-n}(\text{OH})_{n+1(\text{aqu.})} \quad (4)$$

The rate of the dissolution of the hydrated network strongly depends on the number of bridging anions per network-forming cation X. Therefore the corrosion rates of the glasses and the corrosion rates of the grain boundary phases of Si_3N_4 ceramics at least at the beginning of the corrosion process decrease with increasing number of network-forming anions X. If the X-value is low (low number of bridging ions between tetrahedra) in the original glass network then the dissolution process is fast and no or only very thin (nm-thickness) hydrated network layers

are formed. Linear time dependencies of the dissolution can be observed (Figs. 4 and 5). Therefore, the difference between the leaching rates of Y^{3+} and Al^{3+} on the one hand, and the dissolution rate of the hydrated network on the other hand must be quite small for these glasses and a complete dissolution of the glass or grain boundary phase takes place.

The dissolution of a hydrated network depends also on the temperature and acid (H^+) concentration. In addition to the decomposition according to reaction (4), the reverse dehydration reactions of the network takes place to a higher extent in concentrated acids:

$$2 \equiv \text{Si–O–H} \rightarrow \equiv \text{Si–O–Si} \equiv + \text{H}_2\text{O} \quad (5)$$

This reaction results in a decreased solubility of the partial hydrated network and is well known on hydrated silica surfaces and is the reaction converting soluble silicic acid to insoluble silica.[19] This condensation reaction reduces the further destruction of the network and the leaching of the network modifiers. It results in reduction of the corrosion rate or even passivation (Figs. 5 and 6). The hydrated corroded surface layers of glasses are often not very strong and can be easily removed mechanically or by ultrasonic treatment.[4] In the corroded Si_3N_4 ceramics this partially hydrated layer is protected against mechanically removing by the strong Si_3N_4-skeleton and it is stabilised by additional kinetic effects, which become intensified with increasing thickness of the corrosion layer:

1. The reduction of the outward diffusion of dissolved $SiO_2{\cdot}nH_2O$ (or as expressed in Eq. (4). $SiO_{2-n}(OH)_{n+1(aqu.)}$). This is caused on the one side by reduced diffusion cross sections, and on the other side by adsorption of the soluble silicic acid on the surface of the Si_3N_4 grains (a similar effect as used in chromatography).
2. Acceleration of the condensation/dehydration reaction (5) in the corrosion layer reduces the solubility of the partial hydrated network. This reaction is strongly accelerated with increasing $SiO_2{\cdot}nH_2O$-concentration in the solution (reaction is third order in respect to the monomer $SiO_2{\cdot}nH_2O$, i.e. the reaction rate depends on the cube of the concentration of the monomer)[19] and therefore is strongly connected with the first reason. The condensation can take place inside the residual network of the partially dissolved grain boundary, between monomers or between dissolved silicic acids and the surface of the Si_3N_4-grains. All these reactions result in an accelerated formation of the found SiO_2-rich passivating layer.
3. Formation of additional $SiO_2{\cdot}nH_2O$ due to hydrolysis of the Si_3N_4 grains. This factor enhances the effect of the first and second reason. This process is slow, but with increasing thickness of the corrosion layer the surface area in the pores strongly increases and therefore also the overall rate of hydrolysis of the Si_3N_4 grains.

The explained mechanism makes clear that the extended hydrated layers are found only after formation of a corrosion layer with a certain thickness. It explains also that the passivation of the ceramic is faster

- in strong acids (due to stronger polymerisation) (Figs. 2–5);
- in materials with smaller size of triple junctions[4,5] (smaller amount of grain boundary phases or lower grain sizes);
- with increasing temperature from 60 to 120 °C (see Part I). (After Iler the activation energy of the polymerization of silicic acid in acidic media is 96 kJ mol^{-1}.[19] The activation energy of the linear corrosion rate of Si_3N_4 materials was determined as 64 kJ mol^{-1}.[3,5] Therefore, the polymerisation depends stronger on temperature as the corrosion does). The higher concentration of $SiO_2{\cdot}nH_2O$ due to faster corrosion accelerates the dehydration reaction additionally;
- if the corrosion is interrupted by drying[20] at high temperature or oxidation prior to corrosion.[21] This is caused by the strong dehydratisation of the network or forming of SiO_2 glass layer.

The formation of the SiO_2-rich passivating layers does not cause a change to a pure diffusion controlled mechanism (see also kinetic analysis). The diffusion through the layer reduces strongly with the corrosion time resulting in a complete stop of the reaction. Based on the given results it could not be decided which of the dissolved specimens is the one whose rate of diffusion controls the reaction rate—the H^+ ions or the network modifiers. But the mobility of H^+ should be much higher.

The formation of the SiO_2-rich passivating layers reduces the leaching of the network modifiers. This reduction must take place at the interface between the uncorroded microstructure and the passivating layer. The evidence for this is that neither by TEM nor by EDX and WDR gradients of Y and Al were found in the inner corrosion layer.[5,7,8]

The proposed mechanism of the formation of a stable hydrated SiO_2-rich network is also in agreement with the different corrosion behaviour of Si_3N_4 ceramics in HF and under hydrothermal conditions.[4,11,15,24–27]

The process of formation of a stable passivating SiO_2 network in the ceramics is strongly accelerated by an increasing concentration of SiO_2 in the grain boundary of the ceramics (Fig. 13). During corrosion of Si_3N_4-ceramics with medium concentra-

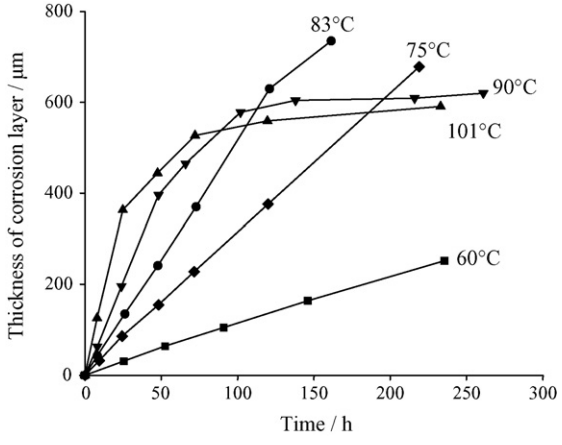

Fig. 13. Time dependent thickness of the corrosion lagers of material KORSiN2a in 0.5 mol/l H_2SO_4 at different corrosion temperatures.

tion of SiO_2 in the grain boundary (medium X-values, material KORSiN9 in 0.5 mol/l H_2SO_4 at 90 °C (Fig. 4)) and in the glass GLAY13 in 3 mol/l H_2SO_4 (Figs. 5 and 6) a formation of a SiO_2-rich layer was also observed. These layers change only the linear corrosion rate but do not result in passivation. The reason for this behaviour has to be investigated more in detail. But one possible explanation could be that on the one hand the formed hydrated network has channels which are large enough to prevent passivation, and on the other hand the network is to stable to permit the formation of additional bridges between the SiO_4-tetrahedron, which would increase the passivating function of the layer.

4.2. Corrosion kinetics

The different structures of the corrosion layers described in the previous chapter result also in different kinetics. The data reveal that different corrosion mechanisms exists and that the mechanisms can change

- with composition of the grain boundary (Fig. 13);
- with changing acid concentration (Figs. 2 and 3) or temperature (Fig. 14).

The different kinetic curves can be divided into five main groups shown in Table 3. The occurrence of the different groups as a function of the materials composition and the corrosion conditions were summarised in Table 4. The kinetic equations given in Table 3 are valid for planar sample geometries. Other sample geometries require more complicated equations[5,22,23] (see also Table 5). For such equations the degree of reaction as a function of time (t) or in our case degree of corrosion α:

$$\alpha = \frac{x(t)}{x(t=\infty)} \tag{6}$$

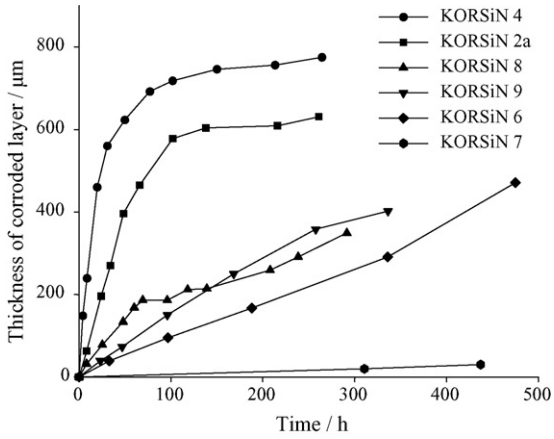

Fig. 14. Time-dependent thicknesses of corrosion layers for various ceramics containing different amounts of SiO_2 in the grain boundary phase at 90 °C in 0.5 mol/l sulphuric acid.

is normally used for the description of the corrosion kinetics, whereas x is the value which changes with the ongoing reaction (in our case weight loss or corrosion layer volume), x at the time $t=0$ is 0 and after complete reaction $x(t=\infty)$ (Table 5). For bending bars made of SN3 the applied models were originally derived for cylindrical samples but can be also used in good agreement for bending bars without producing great errors[22]:

Reaction controlled corrosion:

$$t = (\alpha + (1-\alpha)\ \ln(1-\alpha)b) \tag{7}$$

Diffusion controlled corrosion:

$$t = (1 - \sqrt[2]{1-\alpha})a \tag{8}$$

Mixed reaction control based on (7) and (8):

$$t = (1 - \sqrt[2]{1-\alpha})a + (\alpha + (1-\alpha)\ \ln(1-\alpha)b) \tag{9}$$

with the reaction constants a and b.

Table 3
Types of corrosion kinetics and there characteristic structures (the kinetic equations are valid for planar sample geometry)

Type of corrosion kinetics	Kinetic equation	Characteristics of the corrosion layer	Rate controlling Step
1	Linear: $\Delta x = kt$	Complete dissolution of the grain boundary	Reaction controlled
2	Low t: linear $\Delta x = kt$	Complete dissolution of the grain boundary	Reaction controlled
	Higher t: strong reduction of the corrosion rate to 0	Incomplete dissolution of the grain boundary (hydrated SiO_2 layers)	Passivization due to hydrated SiO_2 layers
3	Low t: $\Delta x = k_1 t$	Complete dissolution of the grain boundary	Reaction controlled
	Higher t: $\Delta x = k_2 t$	Incomplete dissolution of the grain boundary (hydrated SiO_2 layers)	Formed hydrated layer is not passivating
4	$\Delta x = k_2\sqrt{t}$	Nearly complete dissolution of the grain boundary	Diffusion controlled mass transport of dissolved components
5	$\Delta x = k_1 t + k_2\sqrt{t}$	$k_1 t$: reaction controlled decomposition of the hydrated network $k_2\sqrt{t}$: Diffusion of dissolved ions through this corrosion layer	Both mechanisms can superimpose each other before the first terms becomes rate controlling

Table 4
Occurrence of the different corrosion mechanisms

Material	Grain boundary phase	Conditions		Type of corrosion kinetics
		Temperature	Concentration (mol/l)	
All		<60 °C up to 75 °C	0.5	1
Glass	Low and rich on SiO_2; all combinations of Y_2O_3 and Al_2O_3	at 90 °C	0.5	1
		at 90 °C	3	3
All investigated Si_3N_4 ceramics		<60 °C up to 75 °C	0.5	1
SN2, 3		90 °C	≤0.00005	1
SN3	Low SiO_2 concentration and Y_2O_3/Al_2O_3 additives	90 °C	$0.00005 < C < 0.5$	4 or 5
		90 °C	0.05	5
		90 °C	>0.05	2
KORSiN7	SiO_2 rich	>90 °C	0.5	1 or 5
KORSiN8 KORSiN9	Medium SiO_2 concentration	>90 °C	0.5	3
KORSiN2a KORSiN4 KORSiN5	Low SiO_2 concentration	90 °C	0.5	2
SN2	MgAlY containing GB with high SiO_2 content	$60\,°C < T < 90\,°C$	$0.014 < C < 1.5$	1 or 5

Fig. 15 illustrates graphically the results of linear regressions for the SN3 (0.1N H_2SO_4 at 90 °C) expressed in terms of relative corrosion progress according to Eqs. (7) and (8). Despite the good statistical results (Table 5, rows 6 and 7) several facts have to be regarded. Considering the reaction controlled plot it can be recognized that the experimental data are not distributed statistically around the straight regression lines. They show a real curvature and the regression does not match the origin of the graph. A remarkable deviation from linearity is also observed within the first 16 h of the diffusion controlled plot. Better results are obtained from the application of Eq. (9) on the same experimental data as shown in Table 5 and Fig. 16. This model deduced by Frade et al. regards the superposition of a reaction, e.g. an interfacial controlled process and a diffusion controlled process through a distinct layer. Such a situation occurs when both processes have similar reaction rates.

In the following the main figures of the principle corrosion mechanisms (Table 3) will be discussed in relation with the microstructure of the materials and the structure of the formed corrosion layers. As mentioned above these kinetic equations are only valid for planar samples.

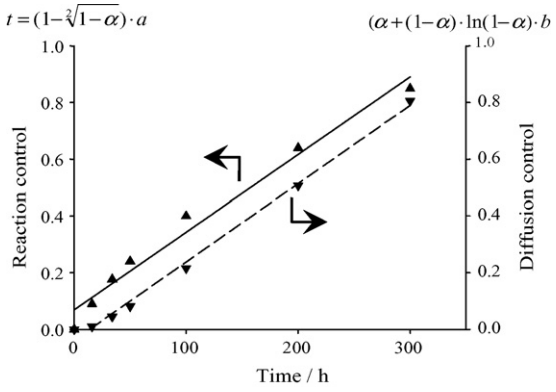

Fig. 15. Results of linear regressions for the SN3 in 0.5 mol/l H_2SO_4 at 90 °C.

Linear time dependencies of the corrosion (e.g. constant corrosion rates) were observed, if a complete leaching of the grain boundary phase was observed. Linear corrosion kinetics are generally explained by the interfacial controlled dissolution of the grain boundary phase.[24–27] The corrosion rate can be explained based on the stability of the oxynitride glassy grain boundary phase and can be directly related to the corrosion rate of the oxynitride glasses with the same composition as the grain boundary (see part 1).[1]

For high corrosion depth and geometries like balls or bending bars the shrinking core effect has to be taken into account. The shrinking core effect results in deviation from the linear time dependence of the weight loss although the thickness of the corrosion layer changes linearly with time. Therefore, measuring of the thickness of the corrosion layer is more useful for the determination of the corrosion mechanism.

In some very stable materials (e.g. SN2) even after 1000 h it cannot be distinguished between the linear law:

$$\Delta m = at + b \tag{9}$$

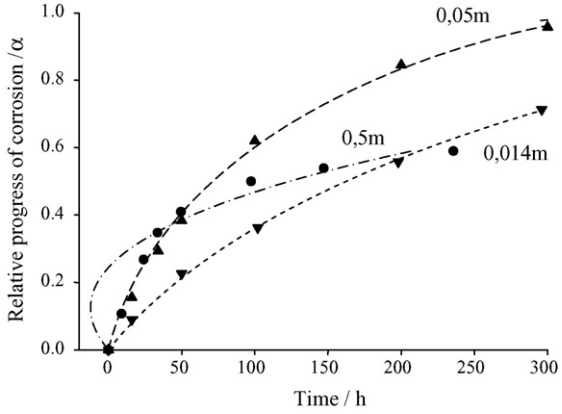

Fig. 16. Graphical representation of the results of the fit of the corrosion kinetic of material SN3 in H_2SO_4 of different concentration at 90 °C; the equation which was used is given in row 8 of Table 4 describes a mixed reaction control.

Table 5
Results of the fitting of kinetic equation to the observed corrosion data

No.	Sample	Model (tab. 2/geometry)	Condition	Equation used	Constants	R^2
1	SN2	1/Planar	0.0014 mol/l H_2SO_4 at 90 °C	$\Delta m = at + b$[a]	$a = 0.15 \pm 0.013\ \mu g\ cm^{-2}\ h^{-1}$, $b = 12 \pm 3\ \mu g\ cm^{-2}$	0.93
2		1/Planar	1.5 mol/l H_2SO_4 at 90 °C	$\Delta m = at + b$[a]	$a = 0.2 \pm 0.018\ \mu g\ cm^{-2}\ h^{-1}$, $b = 18 \pm 1\ \mu g\ cm^{-2}$	0.96
3		5/Planar	1.5 mol/l H_2SO_4 at 90 °C	$\Delta m = at + b\sqrt{t}$[a]	$a = 0.1 \pm 0.05\ \mu g\ cm^{-2}\ h^{-1}$, $b = 3.0 \pm 0.7\ mg\ cm^{-2}\ h^{-0.5}$	0.98
4		5/Planar	0.5 mol/l H_2SO_4 at 90 °C	$\Delta m = at + b\sqrt{t}$[a]	$a = 9.6 \times 10^{-5} + 3 \times 10^{-5}\ \mu g\ cm^{-2}\ h^{-1}$, $b = 2.5 + 0.47\ \mu g\ cm^{-2}\ h^{-0.5}$	0.99
5	SN3[b]	Mixed reaction control/cylinder	0.0014 mol/l H_2SO_4 at 90 °C	$t = (1 - \sqrt[2]{1-\alpha})a + (\alpha + (1-\alpha)\ \ln(1-\alpha)b$	$a = 365 \pm 23$ h, $b = 362 \pm 34$ h	0.99
6		1/Cylinder	0.05 mol/l H_2SO_4 at 90 °C	$t = (\alpha + (1-\alpha)\ln(1-\alpha)b)$	$b = 360 \pm 11$ h	0.99
7		4/Cylinder	0.05 mol/l H_2SO_4 at 90 °C	$t = (1 - \sqrt[2]{1-\alpha})a$	$a = 357 \pm 24$ h	0.98
8		Mixed reaction control/cylinder	0.05 mol/l H_2SO_4 at 90 °C	$t = (1 - \sqrt[2]{1-\alpha})a + (\alpha + (1-\alpha)\ \ln(1-\alpha)b)$	$a = 113 \pm 25$ h, $b = 248 \pm 27$ h	0.99
9		2/Planar	0.5 mol/l H_2SO_4 at 90 °C	$t < 30$ h: $\alpha = at$	$a = 0.01 \pm 0.001\ h^{-1}$	0.99
10	KORSiN2a	2/Planar	0.5 mol/l H_2SO_4 at 90 °C	$t < 50$ h: $\alpha = at$	$a = 0.008 \pm 1 \times 10^{-4}\ h^{-1}$	0.99
11	KORSiN8	3/Planar	0.5 mol/l H_2SO_4 at 90 °C	$t < 60$ h: $\alpha = at$	$a = 0.0027 \pm 0.0001\ h^{-1}$	0.99
				$t > 60$ h: $\alpha = bt + c$	$b = 7 \times 10^{-4} \pm 4 \times 10^{-5}\ h^{-1}$, $c = 0.12 \pm 0.008$	0.98
12	KORSiN9	3/Planar	0.5 mol/l H_2SO_4 at 101 °C	$t < 80$ h: $\alpha = at$	$a = 0.0027 \pm 0.0001\ h^{-1}$	0.99
				$t > 80$ h: $\alpha = bt + c$	$b = 9 \times 10^{-4} \pm 8 \times 10^{-5}\ h^{-1}$, $c = 0.14 \pm 0.015$	0.97
13	KORSiN8	3/Planar	0.5 mol/l H_2SO_4 at 101 °C	$t < 25$ h: $\alpha = at$	$a = 0.006 \pm 0.0005\ h^{-1}$	0.99
				$t > 25$ h: $\alpha = bt + c$	$b = 9 \times 10^{-4} \pm 5 \times 10^{-5}\ h^{-1}$, $c = 0.13 \pm 0.008$	0.99

[a] Due to missing corrosion layers the results were modelled in terms of mass loss
[b] Bar, therefore shrinking core model according to cylindrical geometry.

and the commonly used kinetic equation in glass science

$$\Delta m = at + b\sqrt{t} \quad (10)$$

The first has to be interpreted as the linear corrosion with some surface effects, which can be caused by grinding. The latter law is normally interpreted as diffusion controlled leaching of network modifiers through a hydrated network consisting of network formers (hydrated silica), which decomposes in a reaction controlled manner. With increasing time this hydrated layer determines the corrosion behaviour more and more, and the decomposition of this layer finally becomes the rate controlling step. The thickness of the corrosion layer can range from some nm to μm. For large corrosion times this equation approaches a linear time dependency (Eq. (9)). In Table 5, an example is shown for the corrosion of SN2 in 1.5 mol/l H_2SO_4 at 90 °C.

For the materials with a low SiO_2-concentration in the grain boundary (KORSiN2a, KORSiN4, SN3) the period of a linear time dependence of the corrosion reduces with increasing temperature (Fig. 13). The linear corrosion law is only valid for the starting period of the corrosion under these conditions.

The corrosion of the material SN3 in diluted H_2SO_4 (0.014 mol/l) can be fitted with equations corresponding to diffusion controlled mechanisms. But there are no structural evidences for the determination of the species which controls the reaction (Table 5). With the same accuracy the data can be fitted with equations describing a mixed reaction control.

A more complex situation occurs when product layers are formed. Such layers can be formed by residues of the grain boundary phases in the corroded triple junctions of the Si_3N_4-ceramics. In such cases the corrosion kinetics of Si_3N_4-ceramics, measured in terms of mass loss or thickness of the corrosion layer, strongly deviate from linearity. These layers can be enriched by hydrated SiO_2 as shown in this paper, but also other types of layers could be formed. For example rare earth phosphates can form passivating layers during corrosion of rare earth containing Si_3N_4 materials in phosphoric acid.[2,28] The formation of YF_3 was observed in F^- containing acids.[5,15] The YF_3 precipitations reduce the corrosion rate, but they do not completely suppress the corrosion. The change of the corrosion mechanism strongly depends on the structure of the formed layer:

If the formed layer is still penetrable for the dissolving components as such Y-, Al-cations, this would result in a change to a diffusion controlled mechanism or interfacial corrosion with lower corrosion constant (Glass GLAY13 in Fig. 4; KORSiN8 in Fig. 13; KORSiN8 and KORSiN9 in Table 5).

If the diffusion through the layer slows down more and more, the corrosion reaction will stop and a passivation occurs (Figs. 12–15). The reason for this behaviour was explained in the previous chapter in detail. For such complex corrosion mechanisms a simple equation does not exist to describe the dependence of the thickness of the corrosion layer or mass loss on the time.

In Fig. 16, the experimentally measured degrees of corrosion (volume (corroded)/volume of the sample) are given together with the fitted curves according to the equation in row 8 of Table 5. The bending bars used in the test were approximated as cylinders. Therefore, more complex equations (Table 5) have to be used in comparison to equations in Table 4. The data determined in diluted acids can be fitted well by reactions corresponding to diffusion control or mixed reaction control, whereas the fit of the corrosion data for the samples corroded in 0.5 mol/l H_2SO_4 could not fitted due to the observed formation of passivating layers (Fig. 16).

4.3. Dependence of the corrosion behaviour in H_2SO_4 on the composition of the ceramics

The corrosion stability rises with an increasing SiO_2 content of the grain boundary or more exactly with the increase of the *X*-value (high number of bridging anions). For HIP-SN materials without sintering additives no corrosion attack in HCl-acid was observed.[29]

Materials with low silica contents formed thick corrosion layers within short times and showed a pronounced passivation after formation these layers under certain conditions. Slightly higher silica contents led to slower degradation rates and therefore thinner corrosion layers in comparable times. These materials showed only a moderate slow down of the corrosion rate (Fig. 14; KORSiN8). As the silica content is further increased a change in the corrosion mechanism by means of a deviation from the initial linearity is hardly observed. These results show that a certain thickness of the corrosion layer seems to be necessary to form an efficient protective layer.

The reduction of the amount of sintering additives increases the corrosion resistance in H_2SO_4. Two reasons are responsible for this behaviour:

- with reduced sintering additive content the SiO_2-concentration in the grain boundary phase increases, automatically resulting in more stable grain boundaries.
- with reduced sintering additive content the cross section of the triple junctions reduces causing a faster formation of passivating layers.

The influence of the Al_2O_3-content of the sintering additives on the corrosion resistance is less pronounced than the influence of SiO_2. This has different reasons: Some of the Al_2O_3 is solved in the Si_3N_4 grains reducing the concentration in the grain boundary.[1,2] The remaining alumina in the grain boundary partially works as network-modifying ion, which decreases the corrosion resistance in acids. However Al also can be incorporated into the glass network in a four-fold coordination what in turn results in an increased corrosion resistance. The Al–O bonds inside the glass network show a lower stability than the Si–O bonds. The corrosion rate of YSiAlON-glasses with different Y/Al ratio is shown in Fig. 17.[5] No systematic dependency can be deduced despite of the wide change of the Y/Al ratios, and the corrosion rate can be satisfactorily correlated with the *X*-value (number of network-forming anions per network-forming cation).

Si_3N_4 materials with MgO or MgO/Al_2O_3 sintering additives are considered to be very corrosion resistant.[2,4] This stability

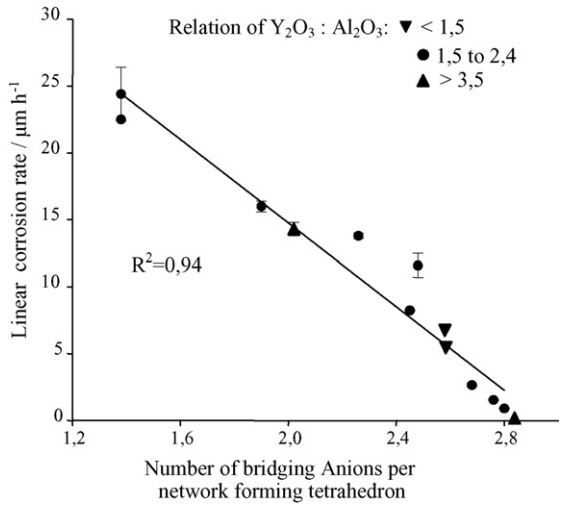

Fig. 17. Correlation between linear corrosion rate constants of YAlSiAlON-glasses in 1N H_2SO_4 at 90 °C and the *X* value (amount of network-forming anions per network-forming cation).[5]

strongly depends on the composition and the corrosion environment. Materials with similar amounts of sintering additives like the Y_2O_3/Al_2O_3–Si_3N_4 ceramics (6–10 vol.%) show similar corrosion behaviour as the Y_2O_3 containing materials.[4] The better sinterability of MgO or MgO/Al_2O_3 cause the lower amount of sintering additives in these Si_3N_4-materials in comparison to the higher amounts which are normally used for Y_2O_3/Al_2O_3-doped materials. Therefore, the reason for the higher stability of MgO or MgO/Al_2O_3 containing Si_3N_4 materials, which is often observed, can be explained by the low additive content and the resulting higher SiO_2-concentration in the grain boundary phase. An additional reason for an improved corrosion resistance can be derived from the glass network theory. The introduction of Mg^{2+} in the network results in a less reduction of bridging anions per network-forming cation in comparison to the introduction of the same amount of Y^{3+}. This explanation of the corrosion stability of MgO/Al_2O_3-containing materials is in agreement with the fact, that these materials are normally less stable in F^- containing media or under hydrothermal conditions.[4,11]

Experiments show that the observed relations between corrosion behaviour and composition of the materials is true also for other acids like HCl, HNO_3, CH_3COOH... The corrosion behaviour is different in acids which can dissolve SiO_2 (e.g. HF) or which form salts with low solubility with components of the grain boundary phase.

5. Conclusions

The investigation of the corrosion behaviour of Si_3N_4 ceramics in H_2SO_4 with different concentrations and at temperatures between 60 and 120 °C showed that both the corrosion rate and the corrosion mechanism strongly depend on the concentration and the temperature of the acid and on the composition of the grain boundary phase.

It is evidenced that the stability of Si_3N_4 materials mainly depends on the composition of the grain boundary phase. The stability of the amorphous grain boundary phase can be described by the number of bridging anions per network-forming cations. Therefore, the materials with the highest amount of bridging anions per network-forming cations in the grain boundary phases (i.e. materials with SiO_2-rich grain boundaries) have the highest corrosion stability in acids like H_2SO_4.

In diluted H_2SO_4 only low corrosion rates are observed which can be described by diffusion, reaction or mixed reaction control. No passivation is observed. A similar behaviour can be found for the corrosion at temperatures less than 60–75 °C.

With an increasing concentration of the acid a passivation is observed at temperatures above 60–75 °C. Therefore, the highest corrosion rates of the Si_3N_4-materials which contain Y_2O_3 and Al_2O_3 as sintering additives can be observed in acids with medium concentrations (range between 0.05 and 0.5 mol/l H_2SO_4) but not in concentrated acids.

The analysis of the corrosion layer has shown that the passivation is caused by the formation of SiO_2-rich layers in the corroded triple junctions. The formation of the passivating layer depends on the SiO_2 content of the initial grain boundary. A corrosion double layer, which is characterized by different amounts of hydrated silica deposits, is observed regularly when a certain thickness of the corrosion layer is reached. However, this double layer is not a direct hint for a passivation under all conditions. Based on the data it could be concluded that at low temperatures and at slow corrosion rates the polymerised structures are not dense enough to suppress the corrosion. A passivating effect is measured when Si_3N_4 materials with a Y_2O_3/Al_2O_3 grain boundary phase and low SiO_2 fractions are corroded at temperatures of 90 °C and higher. Additionally, the concentration of the acids which also influence the polymerisation has to be 0.5 mol/l or higher.

Due to the fact that the passivating layer was observed only after several 100 µm thick corrosion layer this passivating mechanism can not directly be used for an effective passivation of Si_3N_4 materials. The investigations have shown that corrosion resistant Si_3N_4-materials can be reached by tailoring the amount and composition of the grain boundary phase, e.g. after corrosion the material SN2 showed a strength of more than 700 MPa and a corrosion layer thicknesses less than 5 µm).

References

1. Schilm, J., Gruner, W., Herrmann, M. and Michel, G., Corrosion of Si_3N_4-ceramics in aqueous solutions. Part I: Characterisation of starting materials and corrosion in 1 N H_2SO_4. *J. Eur. Ceram. Soc.*, 2006, **26**, 3909–3917.
2. Petzow, G. and Herrmann, M., *Silicon nitride ceramics, structure and bonding*, *vol. 102*. Springer Verlag, Berlin, Heidelberg, 2002, pp. 47–167.
3. Schilm, J., Herrmann, M. and Michael, G., Kinetic study of the corrosion of silicon nitride materials in acids. *J. Eur. Ceram. Soc.*, 2003, **23**, 577–584.
4. Herrmann, M., Schilm, J., Michael, G., Meinhardt, J. and Flegler, R., Corrosion of silicon nitride materials in acidic and basic solutions and under hydrothermal conditions. *J. Eur. Ceram. Soc.*, 2003, **23**, 585–594.
5. J. Schilm, Korrosionsverhalten von Siliciumnitridkeramiken in Säuren, PhD Thesis, Fraunhofer IKTS Dresden and TU Bergakademie Freiberg, 2004.
6. Seipel, B. and Nickel, K. G., Corrosion of silicon nitride in aqueous acidic solutions: penetration monitoring. *J. Eur. Ceram. Soc.*, 2003, **23**, 594–602.
7. Schilm, J., Herrmann, M. and Michael, G., Corrosion of YSiAlON-glasses in acidic and caustic media. *Sil. Ind. Special Issue*, 2004, **69**, 317–324.

8. B. Seipel, Korrosion von Siliciumnitrid und Zirkonoxidverstärktem Aluminiumoxid in Wässerigen Lösungen unter Durchflussbedingungen, PhD Thesis, University of Tübingen, 2003.
9. Somiya, S., Hydrothermal corrosion of nitride and carbide of silicon. *Mater. Chem. Phys.*, 2001, **67**, 157–163.
10. M. Fütting, TEM characterizations accomplished by the Fraunhofer IWM in Halle by order of the Fraunhofer IKTS in Dresden, 2003.
11. M. Herrmann, J. Schilm. and G. Michael, Corrosion behaviour of different technical ceramics in acids, basic solutions and under hydrothermal condition, cfi, 80 (2003) 4, E27–E34.
12. Bando, Y., Mitomo, M. and Kurashima, K. J., An inhomogeneous grain boundary composition in silicon nitride. *Mater. Synth. Process.*, 1998, **6**, 359.
13. Shibata, N., Pennycook, S. J., Gosnell, T. R., Painter, G. S., Shelton, W. A. and Becher, P., Observation of rare earth segregation in silicon nitride ceramics at subnanometer dimensions. *Nature*, 2004, **428**, 730–733.
14. R. Satet, Einfluss der Grenzflächeneigenschaften auf die Gefügeausbildung und das mechanische Verhalten von Siliciumnitrid-Keramiken, PhD Thesis, IKM University of Karlsruhe, 2003.
15. Schilm, J., Herrmann, M. and Michael, G., Leaching behaviour of silicon nitride materials in sulphuric acid containing KF. *J. Eur. Ceram. Soc.*, 2004, **24**.
16. Scholze, H., *Glass—nature, structure and properties*. Springer Verlag, New York, Berlin, 1991, p. 328ff.
17. Risbud, S. H., Analysis of bulk amorphous oxynitride structures using the network theory of glasses. *Phys. Chem. Glasses*, 1981, **22**(6), 168–170.
18. Lemercier, H., Rouxel, T., Fargeot, D., Besson, J.-L. and Piriou, B., Yttrium SiAlON glasses: structure and mechanical properties—elasticity and viscosity. *J. Non-Cryst. Solids*, 1996, **201**, 128–145.
19. R.K. Iler, Chemistry of Silica (Russian Translation), Mir, Mockwa, 1982. 286 ff, 320.
20. Seipel, B. and Nickel, K. G., Protection of silicon nitride ceramics against corrosion in acidic aqueous solutions by enforced internal passivation. *Ceram. Int.*, 2004, **30**(2), 267–271.
21. M. Herrmann, J. Schilm, G. Michael. and J. Adler, Beanspruchungsgerechte Werkstoffoptimierung für korrosionsbelastete großvolumige keramische Elemente für Chemieanlagen auf Basis von LPS-SiC- und Si_3N_4-Werkstoffen, Abschlussbericht zum AiF-Vorhaben 12130 BR (2002).
22. Frade, J. R. and Cable, M., Numerical solutions for mixed control of powder reactions for spherical, cylindrical or planar particles. *J. Am. Ceram. Soc.*, 1995, **78**, 90–96.
23. Frade, J. R. and Cable, M., Theoretical solutions for mixed control of solid state reactions. *J. Mater. Sci.*, 1997, **32**, 2727–2733.
24. Sharkawy, S. W. and El-Aslabi, A. M., Corrosion of silicon nitride ceramics in aqueous HCl and HF solutions at 27–80 °C. *Corr. Sci.*, 1998, **40**(7), 1119–1129.
25. Shimada, M. and Sato, T., Corrosion of silicon nitride ceramics in HF and HCl solutions. *Ceram. Trans. Symp.*, 1989, **10**, 355–364.
26. Sato, T., Sato, S., Tamura, K. and Okuwaki, A., Corrosion behaviour of silicon nitride ceramics in caustic alkaline solutions at high temperatures. *Br. Ceram. Trans. J.*, 1992, **91**, 117–120.
27. Monteverde, F., Mingazzini, C., Giorgi, M. and Bellosi, A., Corrosion of silicon nitride in sulphuric acid aqueous solution. *Corr. Sci.*, 2001, **43**, 1851–1863.
28. Gogozi, Y. G. and Lavrenko, V. A., *Corrosion of high performance ceramics*. Springer Verlag, Berlin, 1992, pp. 76–78.
29. M. Herrmann, A. Krell, J. Adler, G. Wötting, T. Hollstein, W. Pfeifer. and M. Rombach, Keramische Wälzlager für Anwendungen in korrosiven Medien, VDI-Ber. 1331 (Innovationen für Gleitlager, Wälzlager, Dichtungen und Führungen), 1997, pp. 251–258.